

Surface energy partitioning over four dominant vegetation types across the United States in a coupled regional climate model (Weather Research and Forecasting Model 3–Community Land Model 3.5)

Yaqiong Lu¹ and Lara M. Kueppers²

Received 8 October 2011; revised 7 February 2012; accepted 9 February 2012; published 29 March 2012.

[1] Accurate representation of surface energy partitioning is crucial for studying land surface processes and the climatic influence of land cover and land use change using coupled climate-land surface models. A critical question for these models, especially for newly coupled ones, is whether they can adequately distinguish differences in surface energy partitioning among different vegetation types. We evaluated 3 years (2004–2006) of surface energy partitioning and surface climate over four dominant vegetation types (cropland, grassland, needleleaf evergreen forest, and broadleaf deciduous forest) across the United States in a recently coupled regional climate model, Weather Research and Forecasting Model 3–Community Land Model 3.5 (WRF3-CLM3.5), by comparing model output to observations (AmeriFlux, Clouds and the Earth’s Radiant Energy System (CERES), and Parameter-elevation Regressions on Independent Slopes Model (PRISM) data) and to standard WRF model output. We found that WRF3-CLM3.5 can capture the seasonal pattern in energy partitioning for needleleaf evergreen forest but needs improvements in cropland, grassland, and broadleaf deciduous forest. Correcting the leaf area index representation for cropland and grassland could immediately improve the simulation of latent heat flux and hence the energy partitioning. Adding an irrigation scheme is especially important for cropland in the Midwest, where the strongly coupled soil moisture and precipitation can form a positive feedback that reduces latent heat flux and increases the warm bias. For deciduous forest, the simulated excess latent heat flux before leaf emergence is mainly from soil evaporation, requiring further improvement in the soil evaporation scheme. Finally, the domain-wide overestimated net radiation contributes to positive biases in sensible, latent, and ground heat flux, as well as surface temperature. The standard WRF simulation has a similar warm bias, implicating errors in modules other than the land surface code. A sensitivity test suggests that improved simulation of downward solar radiation could reduce the energy flux and temperature biases. After adding irrigation process and correcting the leaf area index, WRF3-CLM3.5 appears reliable for studying conversions between natural grassland and irrigated cropland and between needleleaf evergreen forest and grassland.

Citation: Lu, Y., and L. M. Kueppers (2012), Surface energy partitioning over four dominant vegetation types across the United States in a coupled regional climate model (Weather Research and Forecasting Model 3–Community Land Model 3.5), *J. Geophys. Res.*, 117, D06111, doi:10.1029/2011JD016991.

1. Introduction

[2] A large number of observational and modeling studies have confirmed that the land surface plays a key role in weather and climate [Feddema *et al.*, 2005; Kalnay and Cai,

2003; Pielke *et al.*, 2002, 2007; Pitman *et al.*, 1999; Seneviratne *et al.*, 2006]. The land surface influences the atmosphere through exchange of energy, momentum, water, and CO₂ and other trace gases across the atmospheric boundary layer [Bounoua *et al.*, 2002; Cox *et al.*, 2000]. Conversion from one land cover to another can alter albedo, surface hydrology, boundary layer roughness length, and therefore surface energy partitioning. Moreover, various types of land cover changes can generate quite different climate changes. For instance, conversion of Amazon forest to pasture has significantly increased surface temperature and

¹School of Engineering, University of California, Merced, Merced, California, USA.

²School of Natural Sciences and Sierra Nevada Research Institute, University of California, Merced, Merced, California, USA.

reduced evaporation and precipitation [Malhi et al., 2008; Shukla et al., 1990], while replacing natural grassland with irrigated cropland has introduced much more evapotranspiration and reduced surface temperature [Bonfils and Lobell, 2007; Diffenbaugh, 2009; Kueppers et al., 2007; Lobell et al., 2009]. Even in the absence of irrigation, studies confirm that soil moisture has strong leverage on energy flux partitioning at the surface [Dirmeyer et al., 2000; Guo et al., 2006; Koster et al., 2004].

[3] As climate models become a primary tool for studying the atmospheric role of land surface processes, a question for current climate models is whether they can adequately distinguish and accurately simulate surface energy partitioning over different vegetation types. Plants contribute a large fraction of latent heat flux through evaporation of water from leaf surfaces and transpiration from deeper soil layers when stomata open during photosynthesis. Plants also affect net radiation by altering the surface albedo. A change in plant height can change the boundary layer turbulence by influencing surface roughness, and therefore the total energy exchange via latent and sensible heat fluxes [Davin and de Noblet-Ducoudre, 2010]. In most climate models, several important vegetation parameters (plant function type/vegetation type, leaf area index, stem area index, and canopy top/bottom height) are prescribed according to satellite observations and ground measurements. These parameters are not necessarily accurate at the site scale because of the algorithm and validation methods used in retrieving satellite data or aggregating ground data [Yang et al., 2006]. Validation of surface fluxes over different vegetation types can help identify deficiencies in key parameters and model formulations to target for improving model performance.

[4] Increasing ground and satellite based observations of surface energy fluxes enable validation of energy partitioning in climate models. Ground based networks, such as FLUXNET [Balocchi et al., 2001] and SURFRAD [Augustine et al., 2000] have helped to identify the source of radiation budgets and soil moisture errors [Markovic et al., 2008; Stöckli et al., 2008; Williams et al., 2009]. Satellite derived data, such as International Satellite Cloud Climatology Project [Raschke et al., 2005] and Clouds and the Earth's Radiant Energy System (CERES) [Wielicki et al., 1996] have also been used in model validation [Su et al., 2010; Wild and Roeckner, 2006]. However, many of the validation studies have focused on site averages without considering the vegetation type [Markovic et al., 2008] or a specific vegetation type in the domain, such as tundra in the arctic [Lynch et al., 1999]. The validation of surface energy partitioning over a range of different vegetation types at continental scales has not been generally reported, even though observations suggest that surface energy partitioning varies considerably with vegetation type [Wilson et al., 2002b].

[5] The aim of this work is to examine energy partitioning and surface climate simulated by a recently coupled regional climate model, Weather Research and Forecasting Model 3–Community Land Model 3.5 (WRF3-CLM3.5), for four major vegetation types across the United States, and to identify the model's strengths and deficiencies to help prioritize model improvements. As the next generation mesoscale numerical model, the standard version of Weather

Research and Forecasting (WRF) model includes relatively simple land surface schemes, which potentially constrain model applications for studying the land surface and ecosystem-atmosphere feedbacks. The newly coupled model improved the surface process simulation in California [Subin et al., 2011], but has not been validated at the continental scale. We used the standard version of the WRF model version 3.0 [Skamarock et al., 2008], AmeriFlux site observations (S. C. Wofsy and D. Y. Hollinger, Science Plan for AmeriFlux: Long-term flux measurement network of the Americas, <http://public.ornl.gov/ameriflux/docs/scif.doc>, 1998), and CERES data [Wielicki et al., 1996; Young et al., 1998] to evaluate energy flux partitioning. We analyzed the bias in surface climate variables (daily maximum temperature, daily minimum temperature and precipitation) by comparing to Parameter-elevation Regressions on Independent Slopes Model (PRISM) data sets [Di Luzio et al., 2008]. We focused on four dominant vegetation types with adequate representation in the AmeriFlux network (cropland, grassland, needleleaf evergreen forest and broadleaf deciduous forest).

2. Model and Data

[6] The Community Land Model version 3.5 (CLM3.5) [Oleson et al., 2008] has been coupled into the Weather Research and Forecasting Model version 3 (WRF3) [Skamarock et al., 2008] in an effort to improve simulations of the effects of land cover and land use change on regional climate. Details of the coupling and model validation in California are documented elsewhere [Subin et al., 2011], but will be briefly summarized here.

[7] CLM3.5 represents the surface with five primary subgrid land cover types (glacier, lake, wetland, urban, and vegetated) in each grid cell (the urban subgrid land cover type is not active in WRF3-CLM3.5). The vegetated portion of a grid cell is further divided into patches of up to 4 of 16 plant functional types (PFTs) [Bonan et al., 2002], each characterized by distinct physiological parameters [Oleson et al., 2008]. The spatial distribution of plant function types and leaf area index are obtained from 1 km MODIS observations from 2001 to 2003. Leaf area index (LAI) is prescribed monthly and is updated daily by linearly interpolating between monthly values. The major improvements in CLM3.5 include new surface data sets [Lawrence and Chase, 2007], an improved canopy integration scheme [Thornton and Zimmermann, 2007], scaling of canopy interception [Lawrence et al., 2007], a simple TOPMODEL-based model for surface and subsurface runoff [Niu et al., 2005], a simple groundwater model for determining water table depth [Niu et al., 2007], and a new frozen soil scheme [Niu and Yang, 2006].

[8] We set up two 5 year simulations (2002–2006) for standard WRF3.0.1 and WRF3-CLM3.5, which differed only in the land surface model (Noah versus CLM). The Noah land surface model [Chen and Dudhia, 2001] has 4 soil layers (compared to 10 soil layers in CLM3.5) and only one vegetation type (instead of 4 PFTs in CLM3.5) for each grid cell. There is no separate treatment of shaded and sunlit canopy (CLM3.5 treats shaded and sunlit differently). The other physical packages used in our simulations include the YSU PBL scheme [Hong et al., 2006], the Rapid Radiative

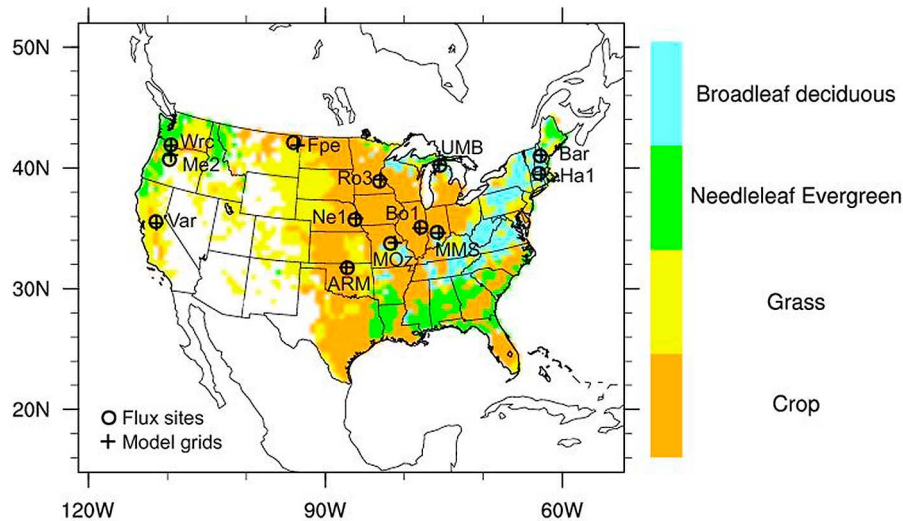


Figure 1. Distribution of the four dominant vegetation types in the model domain. The black circles indicate the AmeriFlux sites used in this work, and plus signs are grid cells nearest to each observation site.

Transfer longwave scheme [Mlawer *et al.*, 1997], the Goddard shortwave radiation parameterization [Chou and Suarez, 1994], the Purdue Lin bulk microphysics scheme [Lin *et al.*, 1983] and the Kain-Fritsch cumulus scheme [Kain, 2004]. These physical configurations yielded the best results for WRF3-CLM3.5 compared to two alternate configurations (one with Duhia shortwave scheme and one with Net Grell cumulus scheme, keeping other schemes the same). We used NCEP/DOE Reanalysis II data as boundary conditions for the period January 2002–December 2006. The simulations focused on the continental United States with 25 vertical layers and 50 km horizontal resolution. We interpolated (using the inverse distance weighting method) 0.5° CLM surface input data (including plant functional types, plant function type percent, leaf area index, and stem area index) into the model domain. For analysis, we removed 8 grid cells from the full perimeter of the domain as a buffer, which diminished the original domain from 109×129 to 93×113 grid cells (Figure 1). We extracted the last 3 years (2004–2006) of output to evaluate model performance over the entire United States relative to ground-based and satellite observations and standard WRF.

[9] As part of the FLUXNET network, AmeriFlux is currently composed of 133 sites (both active and inactive) across North America, Central America and South America. The network collects continuous observations of ecosystem level exchanges of CO_2 , water, energy, and momentum spanning diurnal, synoptic, seasonal, and interannual time scales. Thirteen AmeriFlux sites were used in the analysis. For most comparisons, we used the gap-filled Level 4 database, which has the best quality sensible heat flux (H) and latent heat flux (LE) data. Since lack of energy closure [Wilson *et al.*, 2002a] will affect the magnitude of observed H, LE, and G, we emphasize the Bowen Ratio comparison. Besides the gap-filled Level 4 data, we used Level 2 data with gaps for ground heat flux (G) (only for sites that had $>90\%$ data), net radiation, and radiative fluxes (downward/upward solar and longwave radiation). In addition to the observed energy variables, we examined the three components of modeled latent heat flux: soil evaporation (LESOI),

wet leaf evaporation (LEVEG), and dry leaf transpiration (LETRAN) to diagnose the model deficiencies even though there are no observations of these variables in the flux tower sites.

[10] Although there are a total of 32 sites with Level 4 data from 2004 to 2006, we used only 13 sites (circles in Figure 1) in the analysis after a vegetation type match procedure. Because 50 km resolution and 4 or fewer PFTs per model grid cell are not directly comparable to site-level vegetation types, we assigned all model grid cells to one of four dominant vegetation types (cropland, grassland, evergreen needleleaf forest and deciduous broadleaf forest) according to the plant functional type with the highest percent (and a minimum of 30%) in the grid cell (Figure 1). Even though broadleaf deciduous trees are not $>50\%$ of all BDT grid cells, PFT level fluxes and grid level energy fluxes are very well matched from September to April, and grid level fluxes are only slightly less ($<14 \text{ W m}^{-2}$) than BDT PFT level fluxes in summer. Then for each AmeriFlux site, we selected the nearest model grid cell with the same dominant vegetation type that occurs in the sites (Table 1). Nearest grid cells that were far away ($>100 \text{ km}$) from observation sites were not used.

[11] We interpolated (using the inverse distance weighting method) the CERES monthly TOA/surface mean (SRBAVG) data sets [Wielicki *et al.*, 1996; Young *et al.*, 1998] into our model domain for a continental view of downward solar radiation, upward longwave radiation, and net radiation. CERES is a global satellite product that provides radiation fluxes at top-of-atmosphere and also at the surface (data are available for download at http://eosweb.larc.nasa.gov/PRODOCS/ceres/level3_srbavg_table.html).

[12] We also used PRISM data [Di Luzio *et al.*, 2008] to evaluate the surface climatology (daily minimum temperature, daily maximum temperature, and precipitation). PRISM is recognized as one of the highest-quality spatial climate data sets over the United States. It synthesizes and interpolates point measurements of precipitation, temperature, and other climatic factors to produce continuous, digital grid estimates of monthly, yearly, and event-based climatic

Table 1. Vegetation Composition at AmeriFlux Sites and Corresponding Model Plant Functional Types and Percentages

Site ^a	Site Vegetation	Model PFTs							
		PFT 1	%	PFT 2	%	PFT 3	%	PFT 4/other	%
<i>Cropland</i>									
ARM	Wheat, corn, soybean periodic rotation	Crop	92	BDT Temperate ^b	4	C3 grass	1	Bare Ground	3
Bo1	Corn, soybean annual rotation	Crop	93	BDT Temperate	7	-	-	-	-
Ne1	Maize	Crop	87	C3 grass	7	BDT Temperate	3	Bare Ground	3
Ro3	Corn, soybean annual rotation	Crop	72	C3 grass	16	BDT Temperate	10	Bare Ground	2
<i>Grassland</i>									
Fpe	Grassland	C3 grass	65	Crop	14	BDT Temperate	2	Bare Ground	19
Var	Grazed C3 grassland in a region of savanna	C3 grass	76	NET Temperate ^b	16	BDT Temperate	7	Bare Ground	1
<i>Evergreen Needleleaf Forest</i>									
Wrc	Douglas-fir and western hemlock	NET Temperate	49	C3 grass	36	NET Boreal ^b	12	BDT Temperate	3
Me2	Mature ponderosa pine	NET Temperate	53	C3 grass	33	NET Boreal	8	BDT Temperate	6
<i>Deciduous Broadleaf Forest</i>									
MOz	Oak hickory forest	BDT Temperate	35	Crop	31	C3 grass	25	C4 grass	9
MMS	Mixed hardwood deciduous forest	BDT Temperate	54	C3 grass	24	Crop	20	C4 grass	2
UMB	Deciduous broadleaf forest	BDT Temperate	35	C3 grass	28	NET Temperate	20	Crop	17
Bar	Temperate northern hardwood forest	BDT Boreal ^b	39	NET Boreal	31	C3 arctic grass	29	Crop	1
Ha1	Temperate deciduous forest	BDT Temperate	45	C3 grass	39	NET Temperate	11	Crop	5

^aARM, ARM SGP Main; Bo1, Bondville; Ne1, Mead Irrigated; Ro3, Rosemount G19; Fpe, Fort Peck; Var, Vaira Ranch; Wrc, Wind river crane site; Me2, Metolius Intermediate Pine; MOz, Missouri Ozark; MMS, Morgan Monroe State Forest; UMB, UMBS; Bar, Barlett Experimental Forest; Ha1, Harvard Forest.

^bBDT Temperate, broadleaf deciduous tree-temperate; BDT Boreal, broadleaf deciduous tree-boreal; NET Temperate, needleleaf evergreen tree-temperate; NET Boreal, needleleaf evergreen tree-boreal.

parameters with a 0.05 deg resolution (<http://www.prism.oregonstate.edu>). As with CERES, we interpolated the PRISM data to the model domain for the comparison with model output.

3. Results

3.1. Surface Climate

[13] We compared the 3 year (2004–2006) 2 m daily mean minimum temperature (T_{\min}), daily mean maximum temperature (T_{\max}) and daily mean precipitation to PRISM data. The simulation has a warm bias with regional variation in magnitude. WRF3-CLM3.5 overestimated the T_{\min} (Figure 2a) over all of the United States, especially in the Midwest (>8 K), where most area is covered by crops or grassland. WRF3-CLM3.5's performance is better for T_{\max} (Figure 2b), with most of the West having a smaller warm bias (<4 K) and some mountain areas underestimating the T_{\max} by 4–6 K. For all seasons, the Midwest has a consistent warm bias and the highest warm bias appeared in summer (not shown). Warm biases in the Midwest have also been seen in other combinations of climate and land surface models, such as RegCM-BATS [Walker and Diffenbaugh, 2009] and RegCM-CLM [Tawfik and Steiner, 2011]. WRF3-CLM3.5 underestimated precipitation (Figure 2c) in the Midwest, with some overlap between areas with a dry bias and the warm bias region. Low precipitation may be exacerbating the warmer climate in the overlap region. On the west and east coast, where there is forest cover, the model generally simulated more precipitation than in the PRISM data set.

[14] For the domain mean time series (Figure 2d), the summer has the highest T_{\max} difference, while the T_{\min} bias is consistently large in all seasons (Figure 2d). The large

temperature bias also exists in standard WRF, with reduced summer T_{\max} bias but increased winter T_{\min} bias. Unlike the consistent year-to-year temperature bias, the precipitation bias has more interannual variation. For instance, summer has a large dry bias in 2004 and 2005, but not in 2006 (Figure 2d). Compared to WRF3-CLM3.5, standard WRF shows a greater daily precipitation in nearly all months (Figure 2d).

[15] At the site scale, WRF3-CLM3.5 has a consistent, large warm bias at the 13 flux tower sites in all seasons, with a range from +2.9 to +7.3 K in the monthly mean bias (Table 2) averaged over each vegetation type. Cropland has the highest daily average 2 m temperature (T_2) bias while evergreen forest has the lowest T_2 bias. The daily precipitation bias has more seasonal variation among vegetation types. Generally WRF3-CLM3.5 overestimates the precipitation in winter and underestimates the precipitation in summer (not shown) at the 13 flux tower sites. With respect to monthly mean precipitation, the model simulated too little precipitation for crop and deciduous forest and excess precipitation for grasslands and evergreen forest (Table 2).

3.2. Daily Mean Surface Energy Fluxes

[16] The 13 observation sites we selected capture only a small subset of the area of each dominant vegetation type. Compared to hundreds of model grid cells, most of the observation sites are within the range of the WRF3-CLM3.5 simulation for latent heat flux (LE) (Figure 3a). Modeled sensible heat flux (H) is generally greater than observed (Figure 3b), consistent with WRF3-CLM3.5's warm bias. Flux values at the nearest grid cells tend to be higher than observations for both fluxes for all dominant vegetation types.

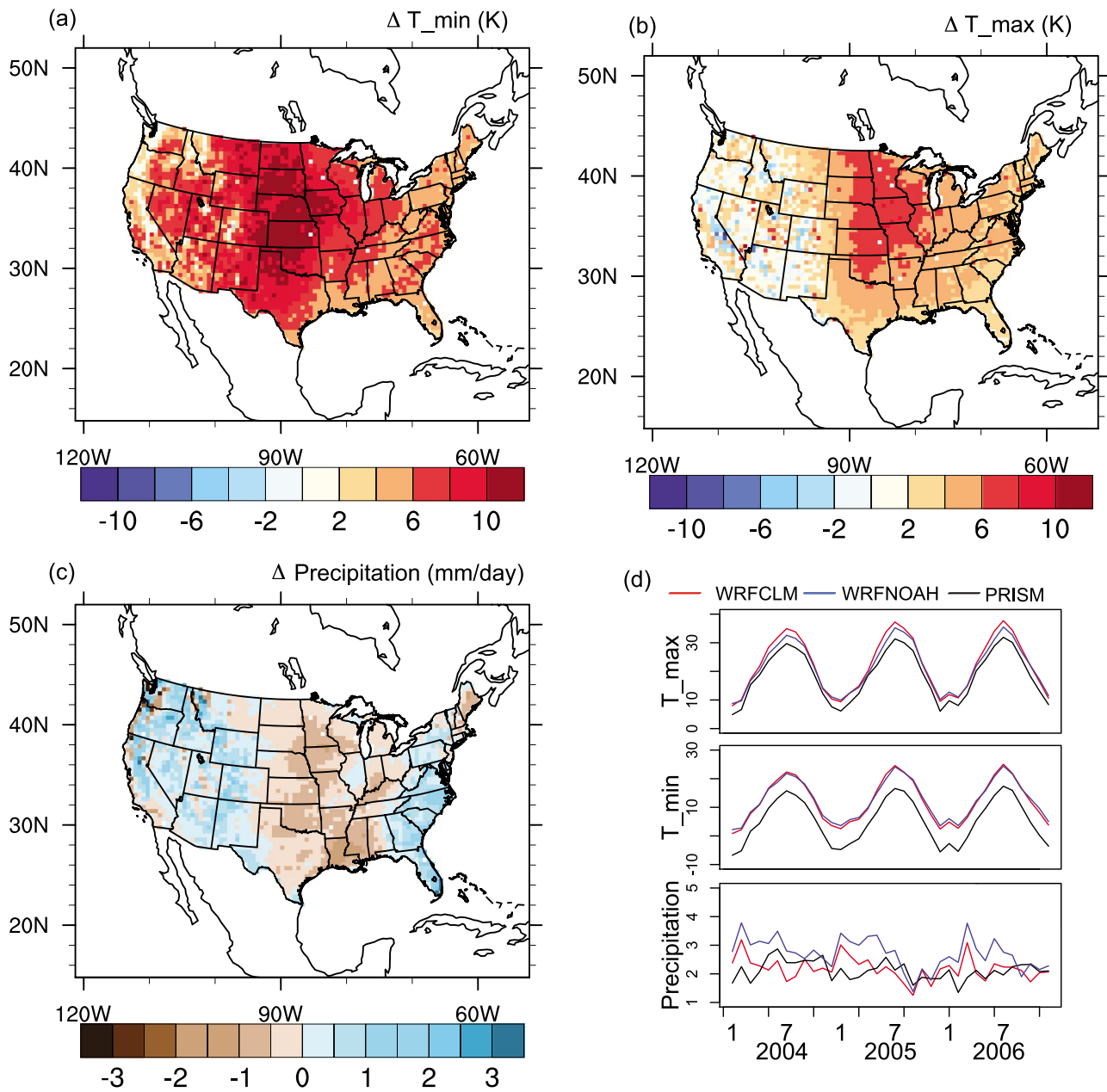


Figure 2. Annual difference in (a) minimum daily temperature, (b) maximum daily temperature, (c) daily precipitation between WRF3-CLM3.5 and PRISM from 2004 to 2006, and (d) monthly time series of T_{max} , T_{min} , and precipitation averaged over the contiguous United States for WRF3-CLM3.5, standard WRF (WRFNOAH), and PRISM.

3.3. Monthly Variation in Surface Energy Partitioning

[17] WRF3-CLM3.5’s performance for monthly partitioning of surface energy is shown for 8 out of the 13 sites in Figure 4, with two representative sites for each vegetation type. Ground heat flux (G) was only available at four sites (Na1, Var, Me2 and MMS) where percent of data available is greater than 90%. Without an irrigation scheme in the model, WRF3-CLM3.5 produced lower LE at irrigated crop site Ne1 while partitioning more energy to H in the summer (Figure 4a). Irrigation at Ne1 results in an observed increase in LE in summer (maximum in August, 114.9 W m^{-2}) corresponding with a decrease in H (minimum in August,

Table 2. Comparison of Annual, Site Level 2 m Temperature, and Daily Precipitation Between WRF3-CLM3.5 (Model) and AmeriFlux (Obs) Averaged for the Four Vegetation Types^a

Site Type	Number of Sites	2 m Temperature (°C)		Daily Precipitation (mm/day)	
		Model	Obs	Model	Obs
Crop	4	19.1 (0.7)	11.8 (0.6)	1.8 (0.4)	2.2 (0.4)
Grass	2	16.2 (0.9)	10.6 (0.8)	2.0 (0.7)	1.4 (0.5)
Evergreen	2	11.5 (0.4)	8.6 (0.5)	5.5 (1.0)	3.6 (1.3)
Deciduous	5	13.7 (0.5)	9.9 (0.5)	2.7 (0.4)	2.8 (0.4)

^aStandard errors of the mean are given in parentheses.

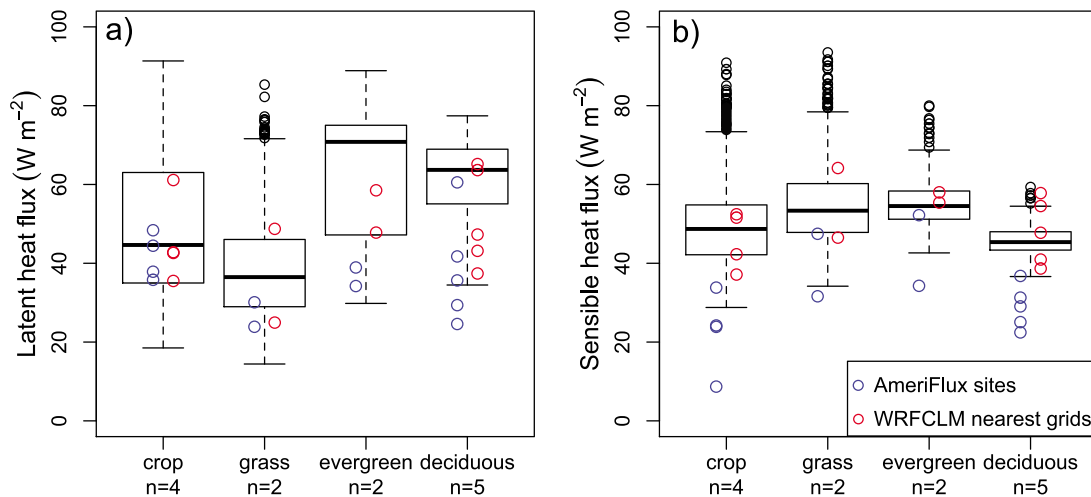


Figure 3. Three years (2004–2006) of daily mean (a) latent heat flux and (b) sensible heat flux for the four dominant vegetation types evaluated. The bottom and top of each box are the 25th and 75th percentile (the lower and upper quartiles, respectively) among all grid cells for the dominant type, and the band near the middle of the box is the 50th percentile. The ends of the whiskers are the lowest and highest data points still within 1.5 times the interquartile range. Black circles are outliers, blue circles are the 3 year daily mean fluxes over 13 AmeriFlux towers (black circles in Figure 1), and red circles are mean fluxes for the grid cells nearest to observation sites (plus signs in Figure 1); “n” indicates the number of observed sites for each vegetation type.

7.8 W m⁻²). However, WRF3-CLM3.5 produced a large H (85.7 W m⁻² in August) and small LE (41.2 W m⁻² in August) in summer. Similar patterns found at two nonirrigated sites (Ro3 and Bo1) could be due to the underestimated precipitation or leaf area index. At the nonirrigated ARM site, the model reasonably simulated monthly variation in H and LE with a slightly higher magnitude than observed (annual average of 17.8 W m⁻² greater H and 6.9 W m⁻² greater LE).

[18] Because of different climate conditions, observed energy fluxes indicate a clear difference in the timing of the growing season at the two grass sites (Figure 4b), which is not replicated by the model. The growing season is spring and summer at Fpe, which has a continental climate, but is winter and spring at Var because of the Mediterranean climate. The growing season usually is associated with large LE because of greater soil evaporation and plant transpiration. The flux tower measurements do show a maximum LE in July at Fpe (86.6 W m⁻²) and in April at Var (63.1 W m⁻²). However, simulated H and LE at Fpe and Var have a very similar temporal pattern (gradually increasing in spring, reaching peak in summer). Such a pattern is reasonable at Fpe but is incorrect at Var where the natural grass has senesced in summer.

[19] For the evergreen forest sites, the energy flux simulations have a pattern similar to the observations, but with greater magnitude (Figure 4c). The annual averaged LE and H differences are 13.6 W m⁻² and 4.8 W m⁻² greater than observed at the Wrc site and 21 W m⁻² and 19.6 W m⁻² greater at the Me2 site.

[20] For the deciduous forest sites (Figure 4d), the flux observations indicated the clear growing season pattern of deciduous broadleaf trees, which was not represented in the simulations. All AmeriFlux deciduous sites observed an LE increase in spring and summer accompanied by a decrease in

summer H when new leaf growth generates stronger photosynthesis and enables more transpiration at the surface. In the simulation, H peaks in the summer season, which is not in agreement with the observation of a peak in March and April before leaf emergence. The same results were observed at the UMBS site for a different time period [Schmid *et al.*, 2003]. At MMS and Ha1, H was correctly simulated before May, but continued to increase and reached peaks in June (Ha1) and August (MMS), while observed H decreased after April. LE was overestimated at Ha1 in most of the months by an average of 18.5 W m⁻² and MMS was overestimated in spring and winter by an average 17.9 W m⁻².

[21] In the model, G is calculated as net radiation (Rn) minus H and LE, therefore errors in Rn, H, and LE could all contribute to the G bias making it hard to diagnose. The simulated G is higher than observations in nearly all months, and the bias magnitude ranges from 1 W m⁻² to 4 W m⁻² over the four sites with adequate data (Ne1, Var, Me2, and MMS, Figure 4 (right)).

[22] The Bowen ratio comparison shown in Figure 5 indicates that the model is good at capturing the monthly partitioning for evergreen forest vegetation, but misses features of the monthly patterns for cropland, grassland, and deciduous forest. For cropland, both WRF3-CLM3.5 and standard WRF overestimated the Bowen ratio (1.3–1.8) because of underestimated latent heat flux. The observed crop Bowen ratio (Figure 5a) was very low (0.26–0.36) between May and September because of increased latent heat flux introduced by irrigation or rainfall. Over the four crop sites, the simulated Bowen ratio from April to September (growing season) was 1.25 for ARM site, 0.75 for Ne1, 0.58 for Bo1, and 0.42 for Ro3. For grassland (Figure 5b), instead of showing the average of the two sites, we plot the Bowen ratios individually since the two sites

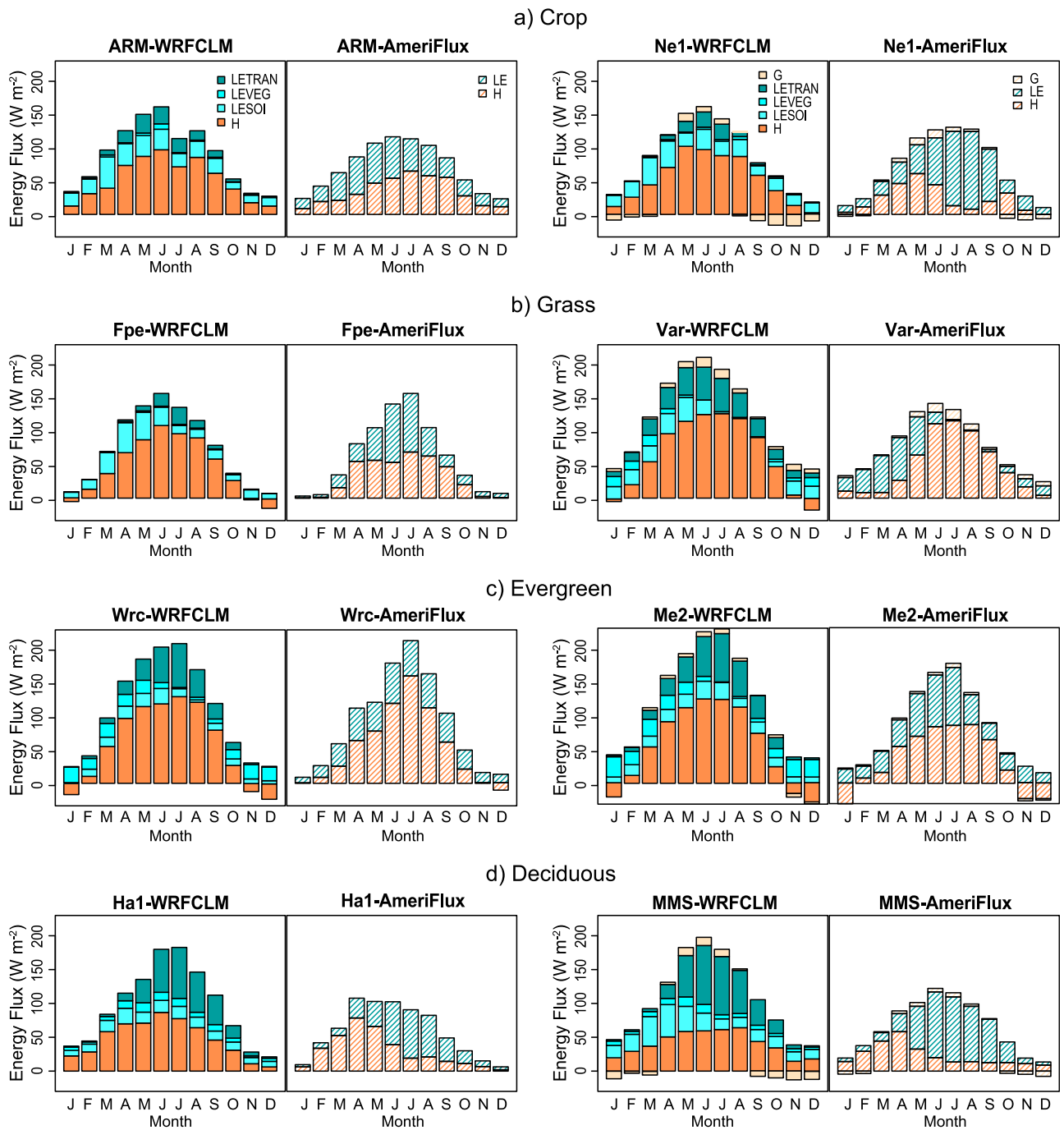


Figure 4. Seasonal energy partitioning (2004–2006 mean) for four dominant vegetation types at eight observation sites (hashed bars) and the nearest grid cells (solid bars). H is sensible heat flux, LE is latent heat flux, LESOI is soil evaporation, LEVEG is leaf evaporation, LETRAN is leaf transpiration, and G is ground heat flux. Observed H and LE are Level 4 AmeriFlux data. G is Level 2 data and only available for select sites.

have very different climates. At the Var site, the observed Bowen ratio is very large (9–21, peak in September) because of little LE and very large H. WRF3-CLM3.5 did not capture the peak while standard WRF overestimates the peak by 13. The large standard errors in the observed summer Bowen ratio realistically reflect the large variation in observed H and LE at the Var site, which suggests challenges for

accurate simulations over grassland areas. The underestimated Bowen ratio by WRF3-CLM3.5 in summer is mainly due to excess LE at the Var site. The source of the incorrect LE can be explained by excess plant transpiration (Figure 4b) due to a too large leaf area index in summer. At the Fpe site, both WRF3-CLM3.5 and standard WRF slightly overestimate the Bowen ratio. For evergreen forest

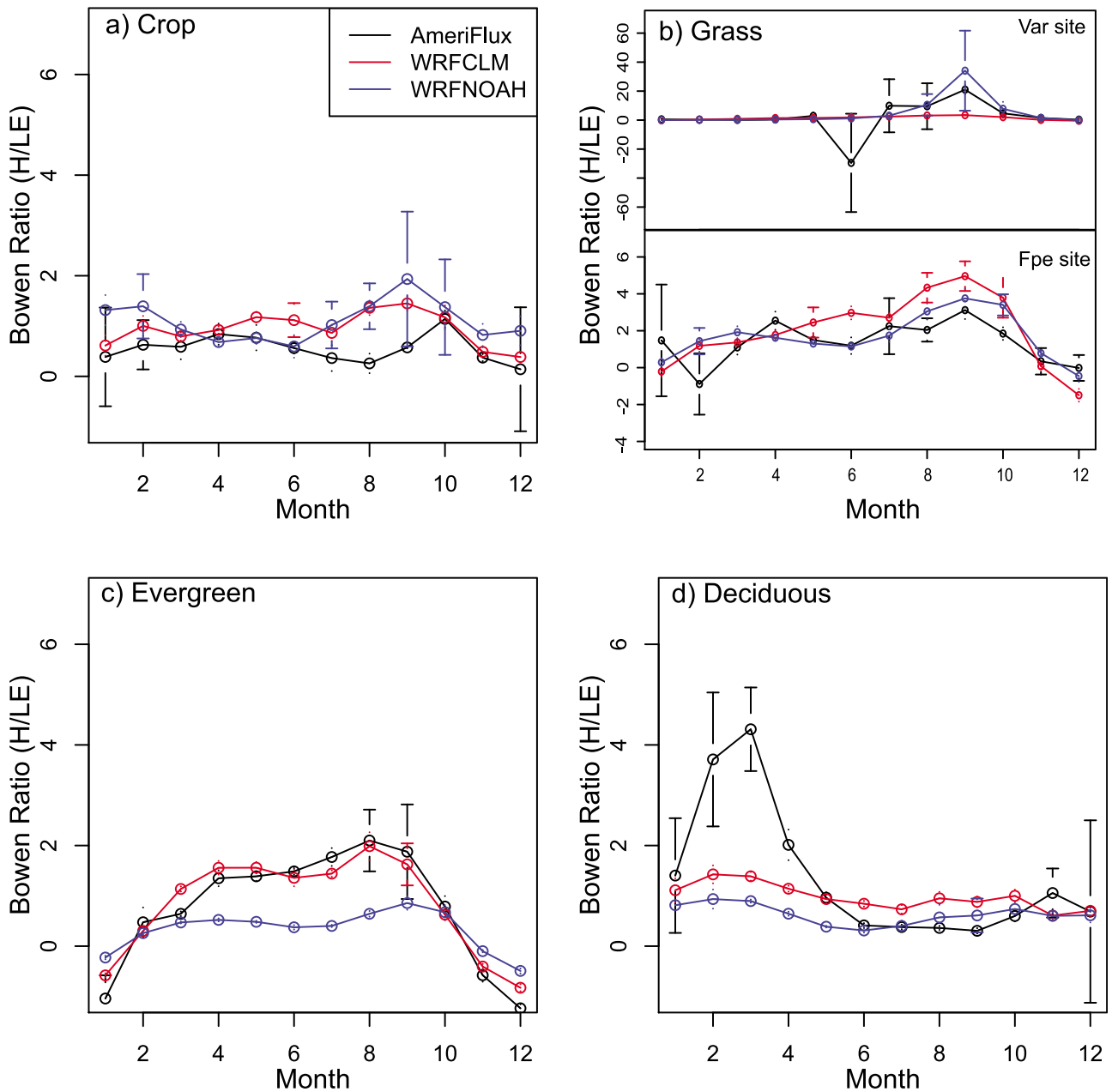


Figure 5. Monthly Bowen Ratio for (a) cropland, (b) grassland, (c) evergreen needleleaf forest, and (d) broadleaf deciduous forest comparing WRF3-CLM3.5 (WRFCLM), standard WRF (WRFNOAH), and AmeriFlux observations. The WRFCLM and WRFNOAH values are the mean of nearest grid cells for each type (plus signs in Figure 1), and the observation values are the mean of the AmeriFlux sites (black circles in Figure 1). The error bars indicate the standard errors ($n = 3$ years). For grassland, instead of showing the average of the two sites, we plot the Bowen ratios individually for Fpe and Far sites since the two sites have very different climates.

(Figure 5c), although the magnitude of the simulated H and LE are both higher than observed (Figure 3), the Bowen ratio matches observations quite well. Notably, the WRF3-CLM3.5 simulation of energy partitioning performs better than standard WRF for evergreen forests in most months. For deciduous forest (Figure 5d), the simulated Bowen ratio is much smaller than observed in spring because of excessive LE (H values are reasonable). Similar to evergreen forest, standard WRF simulated a lower Bowen ratio compared to WRF3-CLM3.5.

3.4. Surface Radiation Budgets

[23] The simulation of surface to atmosphere energy fluxes is highly dependent on the surface radiation budget. Net radiation is the balance between net solar radiation and net longwave radiation. Incorrect simulation of the radiation budget affects the magnitude of the components of the surface energy balance. And in the nonlinear climate system, the magnitude change for H, LE and G may not be the same;

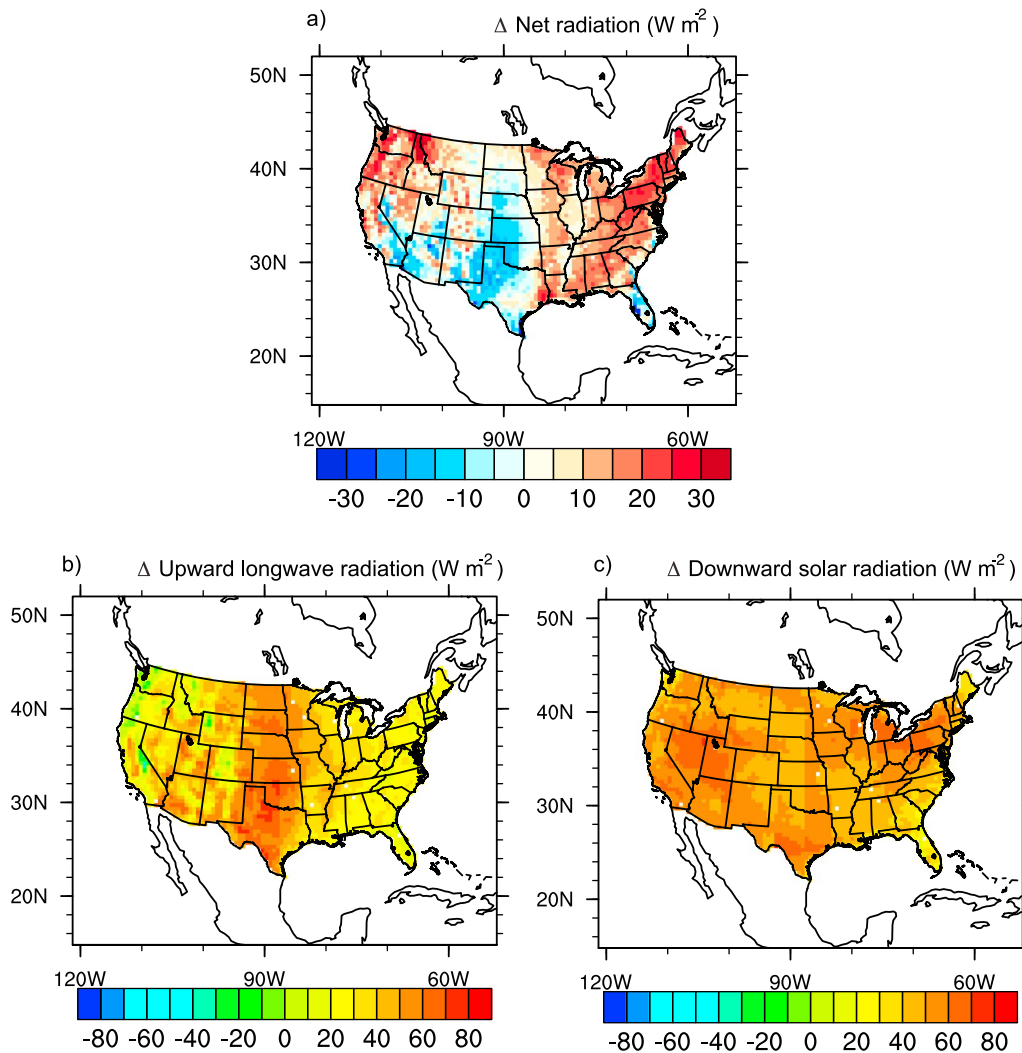


Figure 6. Annual differences between WRF3-CLM3.5 and Clouds and the Earth's Radiant Energy System in 2004 for (a) net radiation, (b) upward longwave radiation, and (c) downward solar radiation.

therefore the bias in the radiation budget could alter surface energy partitioning.

[24] The relatively reasonable simulation of continental-scale net radiation (Figure 6a) is due to two canceling errors. Overpredicted upward longwave radiation (Figure 6b) is canceled by the overpredicted downward solar radiation (Figure 6c). For most regions, the bias in mean net radiation is not large (within $\pm 15 \text{ W m}^{-2}$) compared to the bias in downward solar radiation ($40\text{--}60 \text{ W m}^{-2}$) and upward

longwave radiation ($20\text{--}60 \text{ W m}^{-2}$). In the Midwest, where the warm bias is quite large, the bias in net radiation is actually low (20 W m^{-2}). This is because the higher surface temperature in this region generates higher upward longwave radiation, by 70 W m^{-2} .

[25] At the site level, the model generated 20% or more excess net solar radiation and longwave radiation for all four vegetation types (Table 3), further confirming a systematic overestimation. The excess downward solar radiation for all

Table 3. Surface Radiation Budgets of WRF3-CLM3.5 (Model) (Obs) Over Four Dominant Vegetation Types^a

Site Type	Net Radiation		SW Down ^b		SW Up ^b		Net SW ^b		LW Down ^b		LW Up ^b		Net LW ^b	
	Model	Obs	Model	Obs	Model	Obs	Model	Obs	Model	Obs	Model	Obs	Model	Obs
Crop	88.9	81.7	221.9	191.9	35.2	40.2	186.7	151.7	332.6	371.5	430.4	379.8	-97.8	-8.3
Grass	93.3	59.7	231	183.5	39.2	43.8	191.8	139.7	307.4	302.5	405.9	376.5	-98.5	-74
Evergreen	112.1	90.5	203.6	165.8	23.9	17.8	179.7	148	308.3	304.2	375.9	360.3	-67.6	-56.1
Deciduous	100.5	88.8	209.9	164.6	29.7	23.8	180.2	140.8	320.9	317.8	400.6	371.1	-79.7	-53.3

^aValues for cropland (crop), grassland (grass), evergreen needleleaf forest (evergreen), and deciduous broadleaf forest (deciduous) are the averages over sites for each dominant vegetation type (Table 1).

^bSW Down, downward solar radiation; SW Up, upward solar radiation; Net SW, net solar radiation; LW Down, downward longwave radiation; LW Up, upward longwave radiation; Net LW, net longwave radiation.

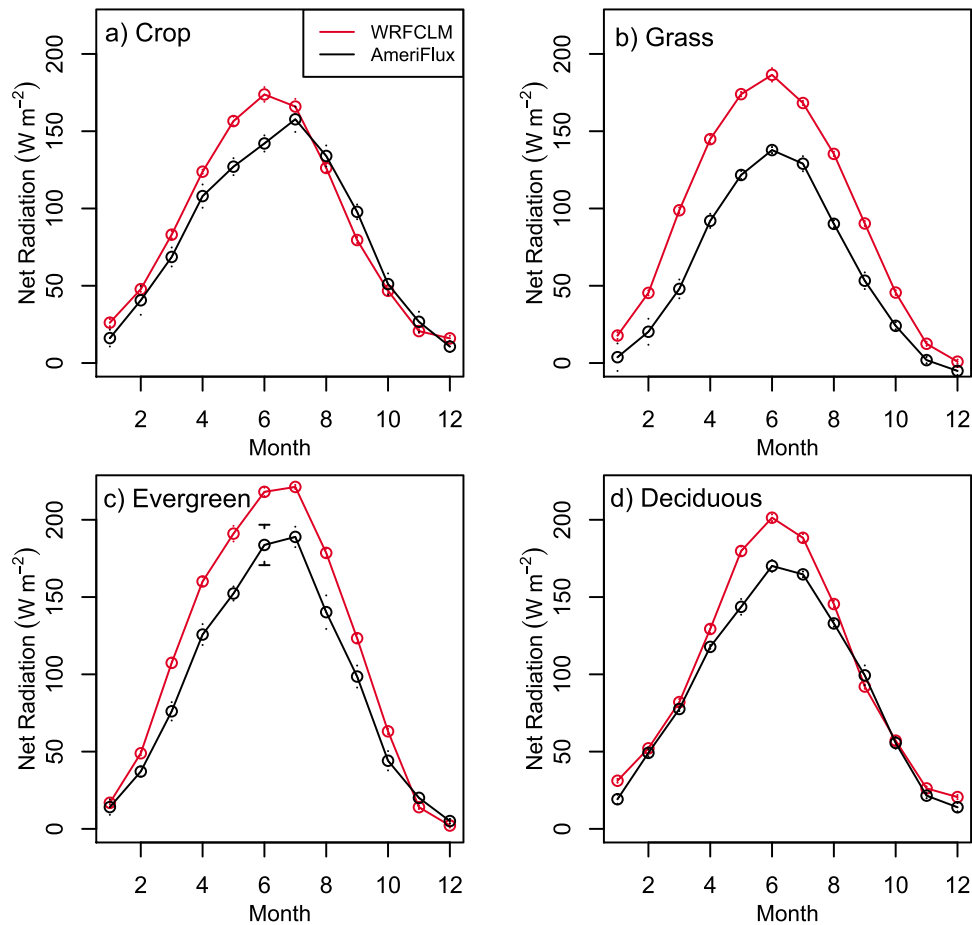


Figure 7. Monthly net radiation for WRF3-CLM3.5 nearest grid cells (red line) and AmeriFlux sites (black line) for (a) cropland, (b) grassland, (c) evergreen needleleaf forest, and (d) broadleaf deciduous forest in 2004.

vegetation types is a discrepancy that has been found in many climate models [Wild, 2008]. We also found that WRF3-CLM3.5 tends to produce a larger downward solar radiation bias in summer than in winter (not shown), which may be due to 20% less cloud cover in summer but not winter (using a rough comparison to CERES cloud cover data, not shown). As would be expected, the model produces excess upward (emitted) longwave radiation because of the overestimated surface temperature. The large bias also dominates the net longwave flux since the bias in downward longwave is negligible except for over crops (Table 3). The temporal variation in the net radiation bias is similar to the downward solar radiation bias: higher in summer than winter (Figure 7), which highlights that downward solar radiation is fundamentally important to correct simulation of net radiation.

4. Discussion

[26] Both WRF and CLM have deficiencies that should be resolved in future versions to reduce the warm bias. The large warm bias in the standard version of WRF suggests there are problems in WRF. For example, the downward solar radiation bias contributes substantially to the warm bias based on a 1 year sensitivity test that artificially reduced

downward solar radiation by 30% (WRF3-CLM3.5 simulated a 3 K lower 2 m air temperature averaged over land grid cells). Reducing downward solar radiation is not simple because it is associated with many factors. Previous work [Markovic *et al.*, 2008; Wild *et al.*, 2001] suggests the overestimate of downward solar radiation at the surface could be either due to less cloud cover for cloudy days or less sky absorption of downward solar radiation for clear days. Ignoring aerosols in the model may also contribute to excess downward solar radiation [Wild, 2008]. The negative precipitation bias in the Midwest (Figure 2c) suggests that an underestimate of cloud cover may contribute to excess downward solar radiation in the Midwest. Further validation with WRF3-CLM3.5 focusing on the cloud cover and clear sky absorption are strongly encouraged but are beyond the scope of this paper.

[27] Fortunately, the newer WRF3.2 includes boundary layer physics and microphysics that could improve the overall simulation. A 1 year sensitivity test using standard WRF3.2 with the MYNN boundary scheme [Nakanishi and Niino, 2009] and Thompson microphysics scheme [Thompson *et al.*, 2008] showed a reduction in the downward solar radiation by 30 W m⁻², in T_{max} by 3 K, and in T_{min} by 2 K.

Table 4. Comparison of Maximum Leaf Area Index Between Model and Observation for AmeriFlux Sites With Measurements (Obs) and Corresponding Model Grid Cells (Model)

Site Type	Maximum Leaf Area Index	
	Model	Obs
Crop ^a	1.91	6.6
Grass ^b	1.4	2.45
Evergreen ^c	4.3	3.62
Deciduous ^d	4.2	4.5

^aCrop, the mean maximum leaf area index at Bo1, Ne1, and Ro3.

^bGrass, the mean maximum leaf area index at Fpe and Var.

^cEvergreen, the mean maximum leaf area index at Wrc and me2.

^dDeciduous, the mean maximum leaf area index at MOZ, MMS, UMB, Bar, and Ha1.

[28] With respect to CLM, the large warm bias in the Midwest could be due in part to (1) the missing irrigation scheme and (2) the lower crop leaf area index used in the model. A large area in the Midwest is covered by irrigated agriculture according to global irrigation maps [Siebert *et al.*, 2005]. Without an irrigation scheme, WRF3-CLM3.5 may overestimate temperature by 3–5 K in summer in the Midwest [Lobell *et al.*, 2009; Sacks *et al.*, 2009]. Considering the strong coupling between soil moisture and precipitation in the Midwest [Koster *et al.*, 2004], low soil moisture could reduce cloud cover and enhance the downward solar radiation, further heating the land surface and contributing to a

positive feedback in this region and producing a large warm bias. Also, the much lower maximum leaf area index used in the model (Table 4) could reduce LE and therefore increase H and near-surface temperature. The simulated seasonal variation in LAI is much lower than the direct measurements at the Bo1 site [Wilson and Meyers, 2007].

[29] Although CLM3.5 includes significant improvements in surface input data [Lawrence and Chase, 2007], there is still space for further improvements because of uncertainties in algorithm and validation methods used to produce the surface data [Yang *et al.*, 2006]. In particular, LAI is a key physiology parameter that strongly influences the LE and surface albedo. With lower LAI, the model may generate lower LE if other conditions remain the same. The lower LE would shift the Bowen ratio, increasing the near surface temperature and even possibly reducing precipitation because of less water vapor transport. For example, the underestimated LE at the Fpe site may be because of the lower LAI used in the model, which is $1.4 \text{ m}^2 \text{ m}^{-2}$ for maximum LAI while the observed LAI is $2.5 \text{ m}^2 \text{ m}^{-2}$ (Table 4). The mean maximum LAI over the crop sites is $6.6 \text{ m}^2 \text{ m}^{-2}$, while the model mean maximum value is $1.9 \text{ m}^2 \text{ m}^{-2}$, which reduced the partitioning to LE in WRF3-CLM3.5. Although the prescribed LAI in the model does not capture the observed interannual variability [Lu *et al.*, 2001], LAI in WRF3-CLM3.5 is quite good for three deciduous sites (Figure 8), where the observed LAI values are similar to the model values. At Ha1, the observed LAI is larger than

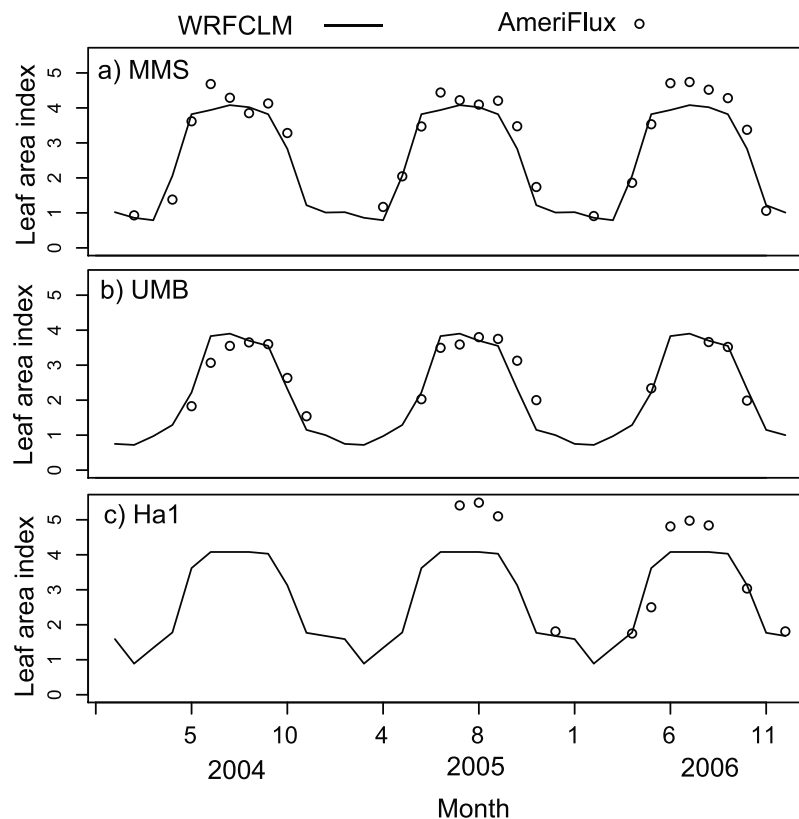


Figure 8. Monthly variation in leaf area index (LAI) for WRF3-CLM3.5 and AmeriFlux observations at three deciduous sites: (a) MMS, (b) UMB, and (c) Ha1. LAI used in WRF3-CLM3.5 is an interpolation of CLM3.5 standard input [Lawrence and Chase, 2007], a prescribed LAI that does not change from year to year (lines). The LAI at AmeriFlux sites are ground observations available for some months (circles).

the model LAI, but the lower LAI in the model yielded a larger LE, which suggests that there are other factors driving the overestimated LE. For instance, the large LE and H in summer may be due to the excess net radiation (Figure 7). Overestimated precipitation in February and March may also help account for the high LE in those months.

[30] In CLM3.5, an additional soil resistance term [Sellers *et al.*, 1992] was added that effectively reduced the unreasonably large soil evaporation in CLM3 [Lawrence *et al.*, 2007]. However, our simulation (Figure 4d) suggests that the excessive soil evaporation is still a problem for broadleaf deciduous forest before leaf emergence in January, February, and March, which is also supported by offline simulations [Stöckli *et al.*, 2008]. At Ha1 and MMS (Figure 4d), it is obvious that the soil evaporation (LESOI) is the largest among the three LE components in spring. The large soil evaporation substantially reduced the Bowen ratio before leaf emergence. The new treatment of soil evaporation in the latest version of CLM [Sakaguchi and Zeng, 2009] reduced the annual average soil evaporation, but mostly in summer in the United States [Lawrence *et al.*, 2011]. Further improvements to reduce spring soil evaporation in broadleaf deciduous regions are highly recommended.

5. Conclusion

[31] Our analyses show that WRF3-CLM3.5 output is in good agreement with observed energy partitioning over needleleaf evergreen forests, but has errors in cropland, grassland and broadleaf deciduous forest. Since none of the current climate models can perfectly simulate energy fluxes and standard WRF has a large wet bias, we believe WRF3-CLM3.5 could be usefully applied in land use conversion research after specific improvements. One recommendation that could immediately improve the simulation is correcting LAI based on available ground observations. For studies focused on the Midwest United States, irrigation processes must be added as in the work of Sacks *et al.* [2009] for a better simulation not only of energy fluxes, but also of temperature and precipitation, because of the strong soil moisture-precipitation feedback. After adding irrigation processes and correcting the LAI, WRF3-CLM3.5 should be reliable for studying conversions between grassland, dryland crops and irrigated crops, or between needleleaf evergreen forest and grassland. Studies involving deciduous forests need to consider the excessive spring soil evaporation that cannot be easily corrected in the current model version.

[32] Our analysis shows that a large warm bias exists both in standard WRF and WRF3-CLM3.5, and that this bias is substantially diminished when downward solar radiation is artificially reduced, suggesting that the WRF model has some deficiencies independent of the land surface model. The very large downward solar radiation in WRF is the driving force for the warm bias, which could be due to too little cloud cover or insufficient sky absorption of downward solar radiation on clear days. Further examination of these potential deficiencies are beyond the scope of this paper, but will be important for improving the quality of regional climate model studies using WRF. A more recent version of WRF includes new schemes for microphysics and boundary

layer physics [Nakanishi and Niino, 2009; Thompson *et al.*, 2008] that also may improve the overall simulation.

[33] **Acknowledgments.** We thank Zachary Subin and Jiming Jin for the original coupling work; the Terrestrial Ecosystems and Climate Policy Working Group funded by the National Center for Ecological Analysis and Synthesis, a center funded by National Science Foundation grant DEB-00-72909; the University of California, Santa Barbara, and the State of California for motivating the simulation; Tom O'Halloran for suggesting the use of flux tower data to validate energy fluxes; Marc Fischer for information on the ARM site; Tilden Meyers for the leaf area information at Fpe and Bon sites; Joseph Norris and Phil Moose for maintaining the El Capitan computing cluster at the University of California, Merced; and three anonymous reviewers for constructive feedback on the manuscript. Both authors were supported by University of California, Merced, for this work.

References

- Augustine, J. A., J. J. DeLuisi, and C. N. Long (2000), SURFRAD—A national surface radiation budget network for atmospheric research, *Bull. Am. Meteorol. Soc.*, *81*(10), 2341–2357, doi:10.1175/1520-0477(2000)081<2341:SANSRB>2.3.CO;2.
- Baldocchi, D., et al. (2001), FLUXNET: A new tool to study the temporal and spatial variability of ecosystem-scale carbon dioxide, water vapor, and energy flux densities, *Bull. Am. Meteorol. Soc.*, *82*(11), 2415–2434, doi:10.1175/1520-0477(2001)082<2415:FANTTS>2.3.CO;2.
- Bonan, G. B., K. W. Oleson, M. Vertenstein, S. Levis, X. B. Zeng, Y. J. Dai, R. E. Dickinson, and Z. L. Yang (2002), The land surface climatology of the community land model coupled to the NCAR community climate model, *J. Clim.*, *15*(22), 3123–3149, doi:10.1175/1520-0442(2002)015<3123:TLSCOT>2.0.CO;2.
- Bonfils, C., and D. Lobell (2007), Empirical evidence for a recent slowdown in irrigation-induced cooling, *Proc. Natl. Acad. Sci. U. S. A.*, *104*(34), 13,582–13,587, doi:10.1073/pnas.0700144104.
- Bounoua, L., R. DeFries, G. J. Collatz, P. Sellers, and H. Khan (2002), Effects of land cover conversion on surface climate, *Clim. Change*, *52*(1–2), 29–64, doi:10.1023/A:1013051420309.
- Chen, F., and J. Dudhia (2001), Coupling an advanced land surface–hydrology model with the Penn State–NCAR MM5 modeling system. Part I: Model implementation and sensitivity, *Mon. Weather Rev.*, *129*(4), 569–585, doi:10.1175/1520-0493(2001)129<0569:CAALSH>2.0.CO;2.
- Chou, M.-D., and M. J. Suarez (1994), An efficient thermal infrared radiation parameterization for use in general circulation models, *NASA Tech. Memo. TM-104606*, 85 pp., NASA, Greenbelt, Md.
- Cox, P. M., R. A. Betts, C. D. Jones, S. A. Spall, and I. J. Totterdell (2000), Acceleration of global warming due to carbon-cycle feedbacks in a coupled climate model, *Nature*, *408*(6809), 184–187, doi:10.1038/35041539.
- Davin, E. L., and N. de Noblet-Ducoudre (2010), Climatic impact of global-scale deforestation: Radiative versus nonradiative processes, *J. Clim.*, *23*(1), 97–112, doi:10.1175/2009JCLI102.1.
- Diffenbaugh, N. S. (2009), Influence of modern land cover on the climate of the United States, *Clim. Dyn.*, *33*(7–8), 945–958, doi:10.1007/s00382-009-0566-z.
- Di Luzio, M., G. L. Johnson, C. Daly, J. K. Eischeid, and J. G. Arnold (2008), Constructing retrospective gridded daily precipitation and temperature datasets for the conterminous United States, *J. Appl. Meteorol. Climatol.*, *47*(2), 475–497, doi:10.1175/2007JAMC1356.1.
- Dirmeyer, P. A., F. J. Zeng, A. Ducharne, J. C. Morrill, and R. D. Koster (2000), The sensitivity of surface fluxes to soil water content in three land surface schemes, *J. Hydrometeorol.*, *1*(2), 121–134, doi:10.1175/1525-7541(2000)001<0121:TSOSFT>2.0.CO;2.
- Feddema, J. J., K. W. Oleson, G. B. Bonan, L. O. Mearns, L. E. Buja, G. A. Meehl, and W. M. Washington (2005), The importance of land-cover change in simulating future climates, *Science*, *310*(5754), 1674–1678, doi:10.1126/science.1118160.
- Guo, Z. C., et al. (2006), GLACE: The Global Land-Atmosphere Coupling Experiment. Part II: Analysis, *J. Hydrometeorol.*, *7*(4), 611–625, doi:10.1175/JHM511.1.
- Hong, S. Y., Y. Noh, and J. Dudhia (2006), A new vertical diffusion package with an explicit treatment of entrainment processes, *Mon. Weather Rev.*, *134*(9), 2318–2341, doi:10.1175/MWR3199.1.
- Kain, J. S. (2004), The Kain-Fritsch convective parameterization: An update, *J. Appl. Meteorol.*, *43*(1), 170–181, doi:10.1175/1520-0450(2004)043<0170:TKCPAU>2.0.CO;2.
- Kalnay, E., and M. Cai (2003), Impact of urbanization and land-use change on climate, *Nature*, *423*(6939), 528–531, doi:10.1038/nature01675.

- Koster, R. D., et al. (2004), Regions of strong coupling between soil moisture and precipitation, *Science*, 305(5687), 1138–1140, doi:10.1126/science.1100217.
- Kueppers, L. M., M. A. Snyder, and L. C. Sloan (2007), Irrigation cooling effect: Regional climate forcing by land-use change, *Geophys. Res. Lett.*, 34, L03703, doi:10.1029/2006GL028679.
- Lawrence, D. M., P. E. Thornton, K. W. Oleson, and G. B. Bonan (2007), The partitioning of evapotranspiration into transpiration, soil evaporation, and canopy evaporation in a GCM: Impacts on land-atmosphere interaction, *J. Hydrometeorol.*, 8(4), 862–880, doi:10.1175/JHM596.1.
- Lawrence, D. M., et al. (2011), Parameterization improvements and functional and structural advances in Version 4 of the Community Land Model, *J. Adv. Model. Earth Syst.*, 3, M03001, 27 pp., doi:10.1029/2011MS000045.
- Lawrence, P. J., and T. N. Chase (2007), Representing a new MODIS consistent land surface in the Community Land Model (CLM 3.0), *J. Geophys. Res.*, 112, G01023, doi:10.1029/2006JG000168.
- Lin, Y.-L., R. D. Farley, and H. D. Orville (1983), Bulk parameterization of the snow field in a cloud model, *J. Clim. Appl. Meteorol.*, 22(6), 1065–1092, doi:10.1175/1520-0450(1983)022<1065:BPOTSF>2.0.CO;2.
- Lobell, D., G. Bala, A. Mirin, T. Phillips, R. Maxwell, and D. Rotman (2009), Regional differences in the influence of irrigation on climate, *J. Clim.*, 22(8), 2248–2255, doi:10.1175/2008JCLI2703.1.
- Lu, L., R. A. Pielke, G. E. Liston, W. J. Parton, D. Ojima, and M. Hartman (2001), Implementation of a two-way interactive atmospheric and ecological model and its application to the central United States, *J. Clim.*, 14(5), 900–919, doi:10.1175/1520-0442(2001)014<0900:IOATWI>2.0.CO;2.
- Lynch, A. H., F. S. Chapin, L. D. Hinzman, W. Wu, E. Lilly, G. Vourlitis, and E. Kim (1999), Surface energy balance on the arctic tundra: Measurements and models, *J. Clim.*, 12(8), 2585–2606, doi:10.1175/1520-0442(1999)012<2585:SEBOTA>2.0.CO;2.
- Malhi, Y., J. T. Roberts, R. A. Betts, T. J. Killeen, W. H. Li, and C. A. Nobre (2008), Climate change, deforestation, and the fate of the Amazon, *Science*, 319(5860), 169–172, doi:10.1126/science.1146961.
- Markovic, M., C. G. Jones, P. A. Vaillancourt, D. Paquin, K. Winger, and D. Paquin-Ricard (2008), An evaluation of the surface radiation budget over North America for a suite of regional climate models against surface station observations, *Clim. Dyn.*, 31(7–8), 779–794, doi:10.1007/s00382-008-0378-6.
- Mlawer, E. J., S. J. Taubman, P. D. Brown, M. J. Iacono, and S. A. Clough (1997), Radiative transfer for inhomogeneous atmospheres: RRTM, a validated correlated-k model for the longwave, *J. Geophys. Res.*, 102(D14), 16,663–16,682, doi:10.1029/97JD00237.
- Nakanishi, M., and H. Niino (2009), Development of an improved turbulence closure model for the atmospheric boundary layer, *J. Meteorol. Soc. Jpn.*, 87(5), 895–912, doi:10.2151/jmsj.87.895.
- Niu, G.-Y., and Z.-L. Yang (2006), Effects of frozen soil on snowmelt runoff and soil water storage at a continental scale, *J. Hydrometeorol.*, 7(5), 937–952, doi:10.1175/JHM538.1.
- Niu, G.-Y., Z.-L. Yang, R. E. Dickinson, and L. E. Gulden (2005), A simple TOPMODEL-based runoff parameterization (SIMTOP) for use in global climate models, *J. Geophys. Res.*, 110, D21106, doi:10.1029/2005JD006111.
- Niu, G.-Y., Z.-L. Yang, R. E. Dickinson, L. E. Gulden, and H. Su (2007), Development of a simple groundwater model for use in climate models and evaluation with Gravity Recovery and Climate Experiment data, *J. Geophys. Res.*, 112, D07103, doi:10.1029/2006JD007522.
- Oleson, K. W., et al. (2008), Improvements to the Community Land Model and their impact on the hydrological cycle, *J. Geophys. Res.*, 113, G01021, doi:10.1029/2007JG000563.
- Pielke, R. A., G. Marland, R. A. Betts, T. N. Chase, J. L. Eastman, J. O. Niles, D. D. S. Niyogi, and S. W. Running (2002), The influence of land-use change and landscape dynamics on the climate system: Relevance to climate-change policy beyond the radiative effect of greenhouse gases, *Philos. Trans. R. Soc. A*, 360(1797), 1705–1719, doi:10.1098/rsta.2002.1027.
- Pielke, R. A., J. Adegoke, A. Beltran-Przekurat, C. A. Hiemstra, J. Lin, U. S. Nair, D. Niyogi, and T. E. Nobis (2007), An overview of regional land-use and land-cover impacts on rainfall, *Tellus, Ser. B*, 59(3), 587–601, doi:10.1111/j.1600-0889.2007.00251.x.
- Pitman, A., R. Pielke, R. Avissar, M. Claussen, J. Gash, and H. Dolman (1999), The role of the land surface in weather and climate: Does the land surface matter?, *IGBP Newsl.*, 39, 4–11.
- Raschke, E., A. Ohmura, W. B. Rossow, B. E. Carlson, Y. C. Zhang, C. Stubenrauch, M. Kottke, and M. Wild (2005), Cloud effects on the radiation budget based on ISCCP data (1991 to 1995), *Int. J. Climatol.*, 25(8), 1103–1125, doi:10.1002/joc.1157.
- Sacks, W. J., B. I. Cook, N. Buenning, S. Levis, and J. H. Helkowski (2009), Effects of global irrigation on the near-surface climate, *Clim. Dyn.*, 33(2–3), 159–175, doi:10.1007/s00382-008-0445-z.
- Sakaguchi, K., and X. Zeng (2009), Effects of soil wetness, plant litter, and under-canopy atmospheric stability on ground evaporation in the Community Land Model (CLM3.5), *J. Geophys. Res.*, 114, D01107, doi:10.1029/2008JD010834.
- Schmid, H. P., H.-B. Su, C. S. Vogel, and P. S. Curtis (2003), Ecosystem-atmosphere exchange of carbon dioxide over a mixed hardwood forest in northern lower Michigan, *J. Geophys. Res.*, 108(D14), 4417, doi:10.1029/2002JD003011.
- Sellers, P. J., M. D. Heiser, and F. G. Hall (1992), Relations between surface conductance and spectral vegetation indexes at intermediate (100 m² to 15 km²) length scales, *J. Geophys. Res.*, 97(D17), 19,033–19,059, doi:10.1029/92JD01096.
- Seneviratne, S. I., D. Luthi, M. Litschi, and C. Schar (2006), Land-atmosphere coupling and climate change in Europe, *Nature*, 443(7108), 205–209, doi:10.1038/nature05095.
- Shukla, J., C. Nobre, and P. Sellers (1990), Amazon deforestation and climate change, *Science*, 247(4948), 1322–1325, doi:10.1126/science.247.4948.1322.
- Siebert, S., P. Doll, J. Hoogeveen, J. M. Faures, K. Frenken, and S. Feick (2005), Development and validation of the global map of irrigation areas, *Hydrol. Earth Syst. Sci.*, 9(5), 535–547, doi:10.5194/hess-9-535-2005.
- Skamarock, W. C., J. B. Klemp, J. Dudhia, D. O. Gill, D. M. Barker, M. G. Duda, X. Huang, W. Wang, and J. G. Powers (2008), A description of the Advanced Research WRF Version 3, *Tech. Rep. NCAR/TN-475 +STR*, Natl. Cent. for Atmos. Res., Boulder, Colo.
- Stöckli, R., D. M. Lawrence, G.-Y. Niu, K. W. Oleson, P. E. Thornton, Z.-L. Yang, G. B. Bonan, A. S. Denning, and S. W. Running (2008), Use of FLUXNET in the Community Land Model development, *J. Geophys. Res.*, 113, G01025, doi:10.1029/2007JG000562.
- Su, W., A. Bodas-Salcedo, K.-M. Xu, and T. P. Charlock (2010), Comparison of the tropical radiative flux and cloud radiative effect profiles in a climate model with Clouds and the Earth's Radiant Energy System (CERES) data, *J. Geophys. Res.*, 115, D01105, doi:10.1029/2009JD012490.
- Subin, Z. M., W. J. Riley, J. Jin, D. S. Christianson, M. S. Torn, and L. M. Kueppers (2011), Ecosystem feedbacks to climate change in California: development, testing, and analysis using a coupled regional atmosphere and land surface model (WRF3-CLM3.5), *Earth Interact.*, 15, 1–38.
- Tawfik, A. B., and A. L. Steiner (2011), The role of soil ice in land-atmosphere coupling over the United States: A soil moisture–precipitation winter feedback mechanism, *J. Geophys. Res.*, 116, D02113, doi:10.1029/2010JD014333.
- Thompson, G., P. R. Field, R. M. Rasmussen, and W. D. Hall (2008), Explicit forecasts of winter precipitation using an improved bulk microphysics scheme. Part II: Implementation of a new snow parameterization, *Mon. Weather Rev.*, 136(12), 5095–5115, doi:10.1175/2008MWR2387.1.
- Thornton, P. E., and N. E. Zimmermann (2007), An improved canopy integration scheme for a land surface model with prognostic canopy structure, *J. Clim.*, 20(15), 3902–3923, doi:10.1175/JCLI4222.1.
- Walker, M. D., and N. S. Diffenbaugh (2009), Evaluation of high-resolution simulations of daily scale temperature and precipitation over the United States, *Clim. Dyn.*, 33(7–8), 1131–1147, doi:10.1007/s00382-009-0603-y.
- Wielicki, B. A., B. R. Barkstrom, E. F. Harrison, R. B. Lee, G. L. Smith, and J. E. Cooper (1996), Clouds and the Earth's Radiant Energy System (CERES): An Earth observing system experiment, *Bull. Am. Meteorol. Soc.*, 77(5), 853–868, doi:10.1175/1520-0477(1996)077<0853:CATERE>2.0.CO;2.
- Wild, M. (2008), Short-wave and long-wave surface radiation budgets in GCMs: A review based on the IPCC-AR4/CMIP3 models, *Tellus, Ser. A*, 60(5), 932–945, doi:10.1111/j.1600-0870.2008.00342.x.
- Wild, M., and E. Roeckner (2006), Radiative fluxes in the ECHAM5 general circulation model, *J. Clim.*, 19(16), 3792–3809, doi:10.1175/JCLI3823.1.
- Wild, M., A. Ohmura, H. Gilgen, J. J. Morcrette, and A. Slingo (2001), Evaluation of downward longwave radiation in general circulation models, *J. Clim.*, 14(15), 3227–3239, doi:10.1175/1520-0442(2001)014<3227:EODLRI>2.0.CO;2.
- Williams, M., et al. (2009), Improving land surface models with FLUXNET data, *Biogeosciences*, 6(7), 1341–1359, doi:10.5194/bg-6-1341-2009.
- Wilson, K., et al. (2002a), Energy balance closure at FLUXNET sites, *Agric. For. Meteorol.*, 113(1–4), 223–243, doi:10.1016/S0168-1923(02)00109-0.
- Wilson, K. B., et al. (2002b), Energy partitioning between latent and sensible heat flux during the warm season at FLUXNET sites, *Water Resour. Res.*, 38(12), 1294, doi:10.1029/2001WR000989.

- Wilson, T. B., and T. P. Meyers (2007), Determining vegetation indices from solar and photosynthetically active radiation fluxes, *Agric. For. Meteorol.*, *144*(3–4), 160–179, doi:10.1016/j.agrformet.2007.04.001.
- Yang, W., et al. (2006), MODIS leaf area index products: From validation to algorithm improvement, *IEEE Trans. Geosci. Remote Sens.*, *44*(7), 1885–1898, doi:10.1109/TGRS.2006.871215.
- Young, D. F., P. Minnis, D. R. Doelling, G. G. Gibson, and T. Wong (1998), Temporal interpolation methods for the Clouds and the Earth's Radiant Energy System (CERES) experiment, *J. Appl. Meteorol.*, *37*(6), 572–590, doi:10.1175/1520-0450(1998)037<0572:TIMFTC>2.0.CO;2.
-
- L. M. Kueppers, School of Natural Sciences and Sierra Nevada Research Institute, University of California, Merced, 5200 N. Lake Rd., Merced, CA 95344, USA.
- Y. Lu, School of Engineering, University of California, Merced, 5200 N. Lake Rd., Merced, CA 95344, USA. (ylu9@ucmerced.edu)